OPTICAL ABSORPTION AND EMISSION FROM RADIATION DEFECTS IN $RbCaF_3$

By

RINA CHAKRABARTI

Bachelor of Arts

University of Calcutta

Calcutta, India

1981

Submitted to the Faculty of the Graduate Collge
of the Oklahoma State University
in partial fulfillment of the requirements
for the Degree of
MASTER OF SCIENCE
December 1985

DEDICATION

To my parents and grandmother-in-law

OPTICAL ABSORPTION AND EMISSION FROM RADIATION DEFECTS IN $RbCaF_3$

Thesis Approved:

W. A. Sibley

I. W. Wilson

E. E. Kohnke

Norman N. Durham

Dean of the Graduate College

ACKNOWLEDGMENTS

I would like to express my graditude to my advisor, Dr. W. A. Sibley for his advice and encouragement during the course of my studies at Oklahoma State University. It has been a priviledge to work for him.

I wish to express my appreciation to Dr. T. M. Wilson for his help and advice.

A note of thanks is given to Mr. Greg Quarles who did the lifetime measurements for me.

Special thanks are given to Dr. L. Feuerhelm, Dr. K. Tanimura, and S. Sibley for their help and friendship.

I extend my thanks to my husband Kishalaya for his useful advice and encouragement.

Finally, I would like to acknowledge Ms. Audrey Brigham for excellence in the typing of this thesis.

TABLE OF CONTENTS

LIST OF TABLES

LIST OF FIGURES

CHAPTER I

INTRODUCTION

Wavelength tunable lasers based on color centers in alkali halide crystals have been developed recently. The new solid-state lasers are gaining increasing importance in research areas such as molecular spectroscopy and fiber optics because of their potential for broadly tunable laser operation in the near-infrared range. These lasers are similar in design to the widely used laser systems based on various dyes in organic solvents. The only difference is in the use of active material which is typically a crystal slab of some material. In some solid state lasers low temperature operation is necessary.

Color center lasers are ionic in nature containing point defects or color centers in which an electron occupies the place of a vacant negative ion (1). This electron is strongly coupled to the lattice vibrations and transitions between these levels produce broad optical bands. Usually color center absorption bands lie in the visible range which is the origin of color in an irradiated crystal and broad emission bands lie in the near-infrared rantge. There is a large frequency shift between absorption and emission bands. The optical transitions can be pumped with appropriate laser sources such as argon or krypton lasers, to produce infrared laser light tunable over most of the spectral width of their emission bands.

The possibility of being used as laser hosts and also information

storage devices in rapidly growing computer technology makes fluoride crystals important. This is the reason they have received much attention lately.

Crystals of $RbMgF_3$ (2-4), $KMgF_3$ (5-7), MgF_2 (8,9), and CaF_2 (10-14), have been investigated widely. The physical properties of those materials can be substantially modified by the presence of impurity ions. Therefore the optical properties of impurities and radiation defects must be studied extensively. Some work has already been done on $RbMgF_3$. This crystal has much promise, but large substitutional impurities such as Er^{3+} and Co^{2+} are too large to substitute in Mg^{2+} sites. Table I provides ion sizes for several different elements.

The size of the Ca^{2+} ion suggests that $RbCaF_3$ might be a useful system which deserves a thorough investigation. In this dissertation we report the optical properties shown by both absorption and emission spectra of radiation induced defects of $RbCaF_3$.

The physical properties of $RbCaF_3$ are listed in Tables II to VII. As Table 2 shows $RbCaF_3$ has a cubic perovskite structure at high temperature (17). This is illustrated in Figure 1.

Some information on the defects in $RbCaF_3$ is available from previous research. It is also possible to identify some radiation induced defects from an analysis of absorption and emission bands attributed to the defects in other materials. The well-known defects produced by radiolysis in alkali halides can be used as a background.

Review of Past Work

Experimental

The defect properties of two important fluoride crystals on which

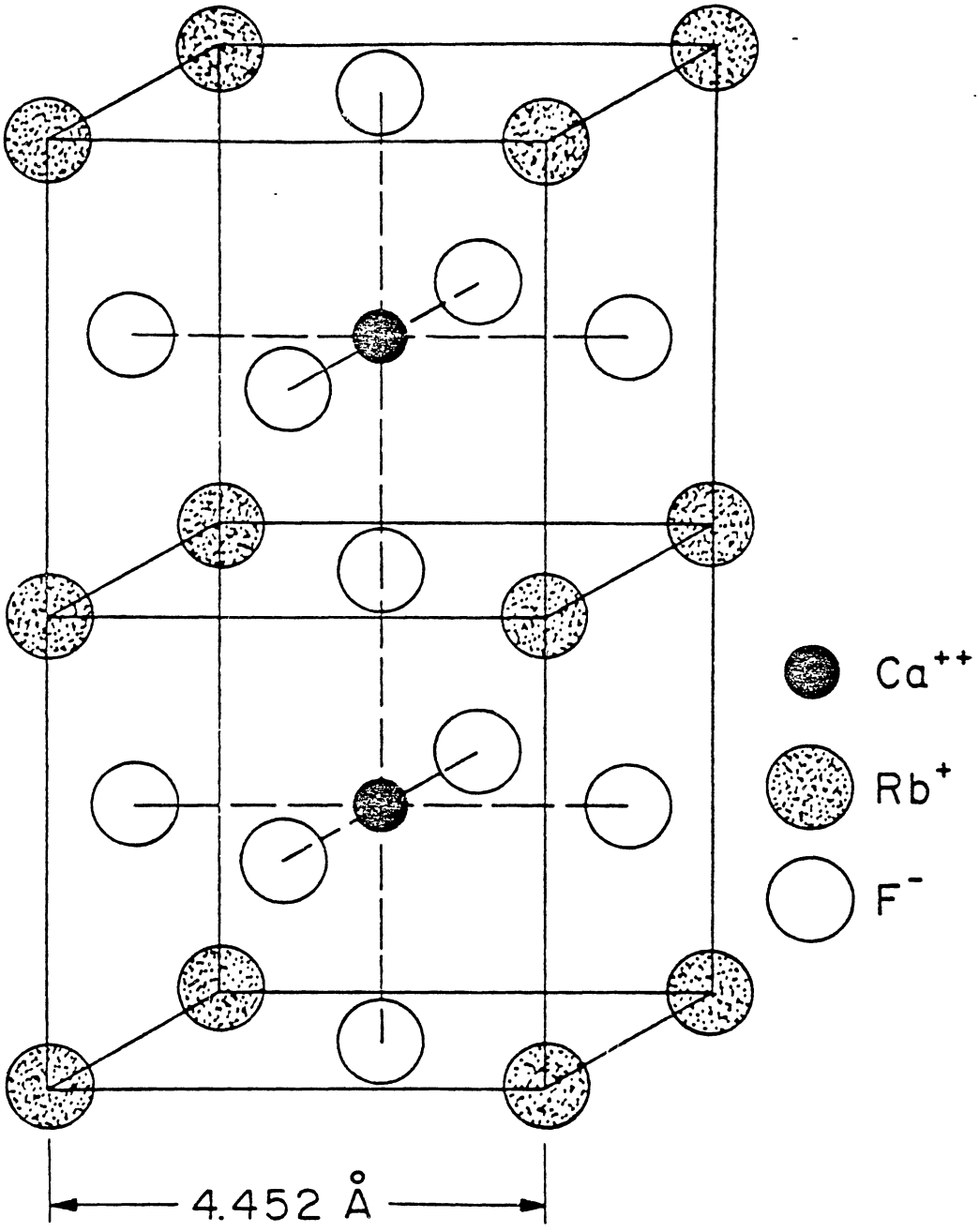

Figure 1. Crystal Structure of $RbCaF_3$

TABLE I

ION SIZES (15)

Ion →	Mg^{2+}	Ca^{2+}	Er^{3+}	Co^{2+}
Radius (A units)	0.65	0.99	1.1	0.72

Sample: $RbCaF_3$

TABLE II

PHASE CHANGE IN CRYSTAL STRUCTURE (16) SPECIFIC HEAT AND LATENT HEAT OF TRANSITION AT DIFFERENT TEMPERATURES.(17)

Temperature range (°K)	Specific heat change ΔC_p (J/gK)	Latent heat of transition (J/mole)	Critical temperature (°K)	Type Transition
80-260	.0062 ± .0004	36	198 + 0.3	cubic to tetragond
30-90	.005 ± .001	7	50.4 ± .8	unknown structural
2-25	-	-	~7	unknown structrual

Density = 3 gm/c.c. (18)
Melting Point = 1110° C (17)

TABLE III

LATTICE PARAMETERS IN DIFFERENT PHASES

Phase →	Cubic	Tetragonal
Lattice parameters	a,b,c	a_t, b_t, c_t
Magnitude	a=b=c=4.452A (19)	$a_t=b_t=\sqrt{2}\ b$ $c_t=2C$ (20)

TABLE IV

THERMAL CONDUCTIVITY AT DIFFERENT TEMPERATURES (16)

TEMPERATURE (°K)	THERMAL CONDUCTIVITY λ (MW/cmK)
1-20	2-20
20-45	20-10
45-500	$10 < \lambda < 100$

TABLE V

OPTICAL BIREFRINGENCE (21)

$(T_c - T)$ (°K)	Birefringence ($x10^{-4}$)
0-120	5-25 (linear rise)

T_c = 198 K
Nature of the sample: Multidomain

TABLE VI

DIELECTRIC CONSTANT AT AUDIOFREQUENCY (10 kHz) (21)

Temperature range (°K)	Dielectric Constant	Transition temperature (°K)
0-20	11.6 - 11.8	
20-25	11.8 - 11.8	25
25-60	11.8 - 13.1	
60-208	13.1 - 12.9	60
208-300	12.9 - 12.6	208

Sample Nature: Polycrystalline

TABLE VII

DIELECTRIC CONSTANT AT MICROWAVE FREQUENCY (9.5 gHz) (21)

Temperature range (°K)	Dielectric Constant E(T)/E(273)	Transition temperature (°K)
0 - 198	0 - 1.009	198
198 - 250	1.009 - 1.001	

much work has already been done are useful for discussion. The first one is CaF_2, one of the main constituents of $RbCaF_3$, and the second one is $RbMgF_3$.

Several radiation induced absorption bands are observed in CaF_2. The energies of these bands are listed in Table VIII. Similar information for $RbMgF_3$ is listed in Table IX.

Color centers or defect centers can be introduced in these ionic crystals by two procedures: (1) heating the material at high temperature near the melting point in the vapor of its constituent metal atom, e.g., vapor of Ca in the case of CaF_2. This process is called additive coloration (22). 2) Irradiation with particles such as electrons, protons, or neutrons. In some cases it is possible to produce color centers in alkali halides with ionizing radiation such as gamma rays or ultraviolet light.

In this study irradiation was employed to produce the defects. Irradiation produces displacement defects such as anion vacancies and interstitial ions. In the case of alkali halides the anion vacancy traps one electron to retain electrical neutrality. An anion vacancy with one trapped electron is called an F-center in alkali halides. Also produced in irradiated alkali halides is the molecular ion defect called the H-center (23, 24). This is an interstitial halide atom bonded with lattice halide ions sharing the lattice sites, the H-center basically consists of an X_2^- molecular ion centered in a single halide-ion vacancy, where x stands for a negative ion. The second type of trapped hole center is $[X_2^-]$ or V_k center (25). This consists of two nearest neighbour <110> halide ions void of an electron (trapped a hole) which combine together to form a $[X_2^-]$ molecular ion. Characteristic spin

TABLE VIII

ABSORPTION AND EMISSION BANDS FOR CaF_2

Defect	Absorption		Emission		Life-time (s)	Temperature (°K)
	Peak(cm^{-1})	Half-width (cm^{-1})	Peak (cm^{-1})	Half-width (cm^{-1})		
V_K (10)	30675	8000	35714	6800		77
V_H (10)	32468	7000	-	-		77
H (11)	33333	7000	-	-		77
F (12)	26596	1.11×10^5	-	-		4
F_2 (12)	19194	4.77×10^5	17065	3.31×10^{-5}	3.8×10^{-8}	20
F_3 (R) (14)	14567	-270.2	14600	~405.4		20

TABLE IX

ABSORPTION AND EMISSION BANDS FOR $RbMgF_3$ (3)

Defect	Absorption		Emission		Temperature
	Peak (cm^{-1})	Half-width (cm^{-1})	Peak (cm^{-1})	Half-width (cm^{-1})	(°K)
V_k	30303	7655.1	-	-	300
F	33898 30769	6098 4791	-	-	300
$F_2(M)$	25840	1813	23256	2659	300
$F_3(R)$	33333	2417	30303 20408	7252 2417	10 300

resonance spectra (26,27) and optical absorption spectra (28,29) have been observed for these so-called self-trapped holes. In the case of H center defects, there are more ions than in corresponding lattice sites, whereas for $[X_2^-]$ hole trap centers, the two anions have two lattice sites. Both V_K and H centers are observed at low enough temperature. The structure of the F-centers and H-center in $RbCaF_3$ are illustrated in Figure 2 and in Figure 3 respectively.

When irradiations are made at liquid helium temperature all defects are immobile after creation. However, at temperatures nearer 300 K first H-centers, then $[X_2^-]$ center and finally F^+ centers become mobile. As each of these defects become mobile the radiation damage process is affected (24). In most halides the interstitial atom, the H-center, becomes mobile before the F. As it does so, it can recombine with vacancies or be trapped by impurities and other interstitials. Similar events occur when vacancies become mobile which happens at higher temperatures than for interstitials. These vacancies aggregate to form F_2 and F_3 centers. They can annihilate interstitials or be trapped by impurities. Since interstitials cluster even at low temperatures (31), when vacancies do eventually become mobile only other vacancies and impurities are widely distributed in the lattice. This means that moving vacancies are much more likely to interact with impurities (to form F_A or Z like centers) and with other vacancies (to form F aggregate centers) than with interstitials.

One of the most important effects of the radiation damage process in alkali halides arises from the behavior of holes and of non-radiative electron hole recombination, because the hole (or $[X_2^-]$ center) is the the precursor of the photochemical damage process. Thus at low

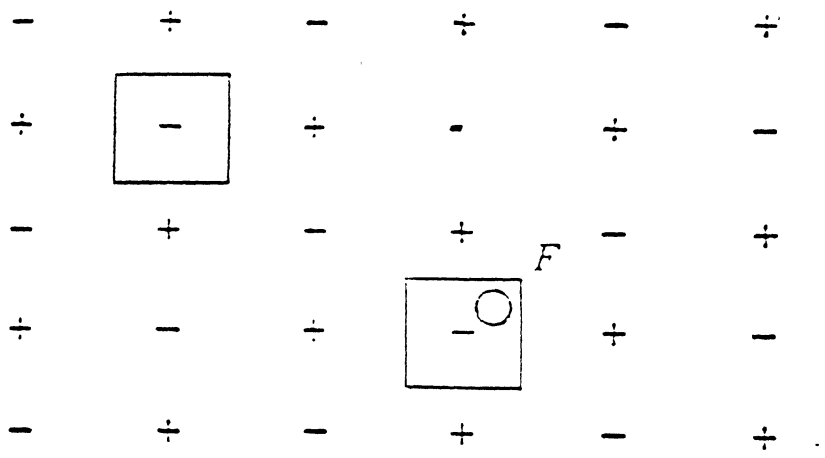

Figure 2. Schematic Diagram Showing an Anion Vacancy and an Anion Vacancy with Electron Trapped in it; the Latter is Known as an F Center

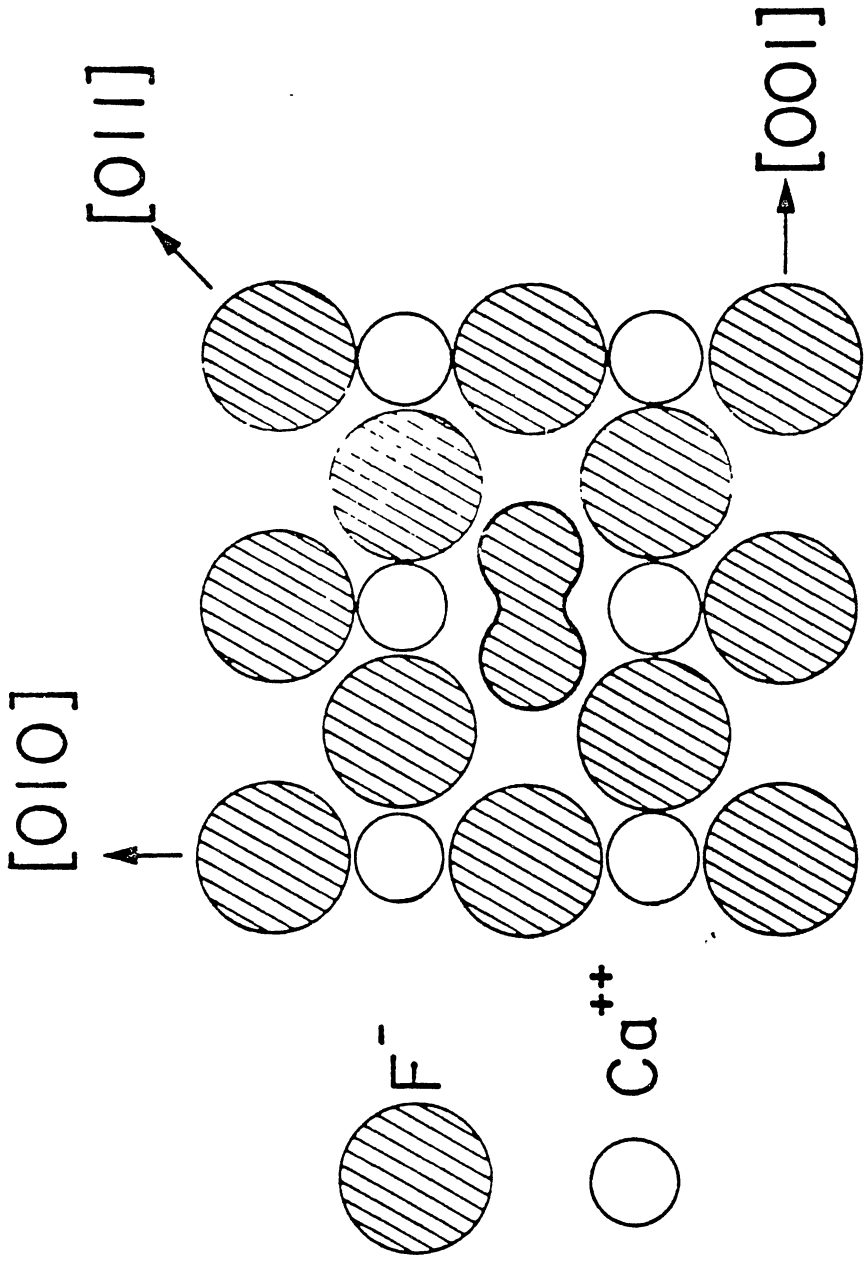

Figure 3. Model for the H Center in $RbCaF_3$

temperatures coloration is often suppressed because radiative recombination predominates over non-radiative (32). At high temperatures $[x_2^-]$ centers become mobile and are able to move through the lattice and recombine with electrons at impurities rather than in undisturbed lattice. When this happens, the production process is inhibited (33,34).

Theory

The general theory of atomic emission and absorption involves the calculation of certain integrals known as matrix elements. The matrix element involved in electric dipole radiation is the quantity M_{AB} defined as

$$M_{AB} = \Sigma \int U_A^* \, e \, \vec{r}_s \, u_B \, d_q$$

where $\vec{r}=x\hat{i} + y\hat{j} + z\hat{k}$ and e is the electric charge. The dipole matrix element is a measure of the amplitude of the oscillating dipole moment of the coherent state formed by two stationary states U_A and U_B with energies E_A and E_B respectively. The summaion is taken over all electrons.

If a monochromatic beam of N photons per unit volume, each of energy $h\omega$, impinges upon an atom, the probability per unit time W_{BA} that the atom will make a transition from state B to state A is given by,

$$W_{BA} + \frac{4\pi^2 |E_B - E_A|}{h} N \, | \, \hat{\eta} \, \bar{M}_{AB}|^2 \, \delta(|E_A - E_B| - h\omega) \qquad (1)$$

Here $\hat{\eta}$ is a unit vector denoting the polarization of the incident

light. If the beam is unpolarized, we may write,

$$\text{Avg} \mid \hat{n} \cdot \bar{M}_{AB}\mid^2 = \frac{e^2}{3}[x_{AB}^2 + y_{AB}^2 + Z_{AB}^2] = \frac{1}{3}\mid\bar{M}_{AB}\mid^2 \tag{2}$$

and express the transition probability as

$$W_{BA} = \frac{4\pi^2\mid E_A - E_B\mid}{3h} N\mid M_{AB}\mid^2 \delta(\mid E_A - E_B\mid - h\omega) \tag{3}$$

The above equations are valid under these circumstances: (1) the photon density N is small; and only processes linear in N are considered, (2) before the transition, the probability that the atom was in state B is 1; (3) the transition effectly involves the dipole transition; thus the selection rules hold, (4) both A and B are discrete states.

There are several other quantitites which are directly related to W_{BA}. One of the most important of them is the absorption cross-section Σ_{BA} . This can be defined as the transition probability divisded by the photon flux and integrated over the energy delta function (Dexter, 1958):

$$\Sigma_{BA} = \int \frac{W_{BA}}{Nc}\, d(h\omega) \tag{4}$$

or,

$$\Sigma_{BA} = \frac{4\pi^2 h\omega_{AB}}{3hc}\mid\bar{M}_{AB}\mid^2 \tag{5}$$

where $h\omega_{AB} = \mid E_A - E_B\mid$. Σ has the dimensions of (area) times (energy).

At this point we can introduce a dimensionless quantity called

"oscillator strength", a tensor that in many cases reduces to a scalar.

$$f_{BA} = \frac{2m}{3he^2}\,\omega_{BA}\,|\bar{M}_{AB}|^2 \qquad (6)$$

The oscillator strength enters as a correction to the classical Lorentz theory of the electron. In general, it satisfies the sum rule:

$$\sum_k f_{mk} = 1$$

where the summation is over all states k.

This oscillator strength gives us an important relationship called Smakula's formula. In this formula, the number of centers N, the oscillator strength f, maximum absorption coefficient α_{max} and half-width W of the absorption band are related in the following way:

$$Nf = 0.87 \times 10^{21}\,\frac{\eta}{(\eta^2+2)^2}\,\alpha_{max} W \qquad (7)$$

where η is the refractive index at the peak of the band. In this relation, N is in per m^3, α_{max} is in m^{-1} and W is in eV. The above relationship is only valid for absorption bands which have a Gaussien shape as most color centers do. For allowed dipole transitions f is always near unity; more specifically, it is about 0.7 for F bands in alkali halides. Again for alkali halides, $\eta \sim 1.5$ and $W \sim 0.5$ eV for F centers so that

$$N_F = 10^{16}\alpha_{max}$$

where N_F is the concentration of F-centers in cm^{-3}.

This method is a very powerful tool to determine the concentration of defect centers. Once we identify the bands due to particular defects centers, we can construct gaussian fits for these bands and we can calculate the oscillator strength as well as the concentration of defect centers using the above relationships.

CHAPTER II

EXPERIMENTAL PROCEDURES

The crystals used in this study were grown at the Oklahoma State University Crystal Growth Facility. Growth procedures for the samples of $RbCaF_3$ are described by Seretlo et al.(18). Samples were cut with a diamond saw and polished by hand lapping on successively finer sheets of abrasive obtained from Buehler, Ltd. Thickness of the sample was measured in several places with a micrometer screw. An average of 9 readings was taken to determine the thickness of the sample.

As we have seen in Chapter I, $RbCaF_3$ has a cubic pervoskite crystal structure at high temperature. A cubic-to-tetragonal phase change occurs at 198K. To check the orientation of the crystal c-axis He-Ne laser and crossed polarizers were used. Polarized light was obtained through the use of glan polarizers or polaroid type HNP'B ultraviolet sheets. The sample was placed such that light enters the crystal perpendicular to a face presumed to be along a <001> direction because of cleavage. At room temperature, the sample is cubic, therefore light can be extinguished by crossed polarizers. When the sample is below 198K, one of three directions will become the c-axis. If the c-axis is parallel to the direction of light, light is still extinguished. If the c-axis is perpendicular to the light, the light will be somewhat polarized (rotated) by the crystal, and is no longer extinguished on the screen. By testing all three axis one by one, the crystal c-axis was

identified to be along the horizontal surface of the sample

For low temperature measurements, a sulfrian helium cryostat, or CTI cryodyne cryocooler Model 21SC was utilized. The cryogenerator was equipped with a resistance heater which allowed temperature control within ± 1K over the range 14 - 300 K. The temperature was monitored with a gold-iron vs chromel thermocouple mounted on the cold finger just above the sample.

The samples were irradiated with 1.70 MeV electrons through a 0.25 - mm Al window. The Oklahoma State University Van de Graff accelerator was used for irradiation. The distance between the sample and the accelerator window was 10 cm. The irradiations were done at 3 μA at a dose rate of 2.3×10^{13} MeV/cm^3-sec measured in air using a Ag-glass dosimeter.

Optical absorption was measaured using a Perkin-Elmer 330 spectrophotometer which records the optical density of the sample as a function of wavelength. The optical density is given by, O.D. = $\log_{10}(I_o/I)$, where I_o and I are the intensities of the reference and sample beams respectively. The optical density is related to the absorption coeffiecient (α) by the relation

$$\alpha = 2.303 \text{ (O.D./t) cm}^{-1}$$

where t is the sample thickness in cm.

Optical bleaching was carried out by illuminating the sample from an Illumination Industries 300-W xenon-arc lamp. This light was focused with a quartz lens and rendered monochromatic by passing it through a SPEX Industries, 22 cm monochromator.

Luminescence measurements were made using the apparatus shown schematically in Figure 4. The exiting light source was a 300-watt

short arc xenon lamp from Illumination Industries passed through s SPEX industries, Inc., 22 cm Minimate monochromator. The grating used in the Minimate has specifications of 1200 gr/mm with a reciprocal dispersion of 4 nm/mm and was blazed at 300 nm. The light was chopped by a Keithley Model 8403-450 light chopper at a frequency of 450 Hz. The chopped light was reflected with a front surface mirror onto the front surface of the sample, which had been rotated slightly off of a 45° angle to minimize the amount of exiting light reflected into the detection system. The fluorescnece was focussed with calcium fluoride lenses into a 0.8m SPEX 1702 monochromator which has a 600 gr/mm grating blazed at 1600 nm with a reciprocal dispersion of 2 nm/mm. It was detected with an RCA C31034 photomultiplier tube cooled with a Pacific Photometrics Model 33 thermoelectric cooler. The cooling allowed the photomultiplier tube to be operated at 1800V DC without excessive dark current. The signal from the PMT was preamplified by a Keithley Model 427 current ampliflier and passed to the lock-in amplifier. The reference signal was provided by a photodiode placed at the edge of the exiting light, which was modulated by a variable speed, single hole chopper. The output of the lock-in amplifier was displayed on a Houston Instruments 2000 x-y recorder, or routed to a Hewlett-Packard model 3455A digital voltmeter which was interfaced to a Hewlett-Packard Model 85 microcomputer. This allows excitation or emission spectra to be recorded on disc for further processing.

To correct the emission spectra a General Electric QL-157 quartz-iodine standard lamp, whose characteristics are traceable to the National Bureau of standards was used. Finally all data were corrected for excitation intensity and system response.

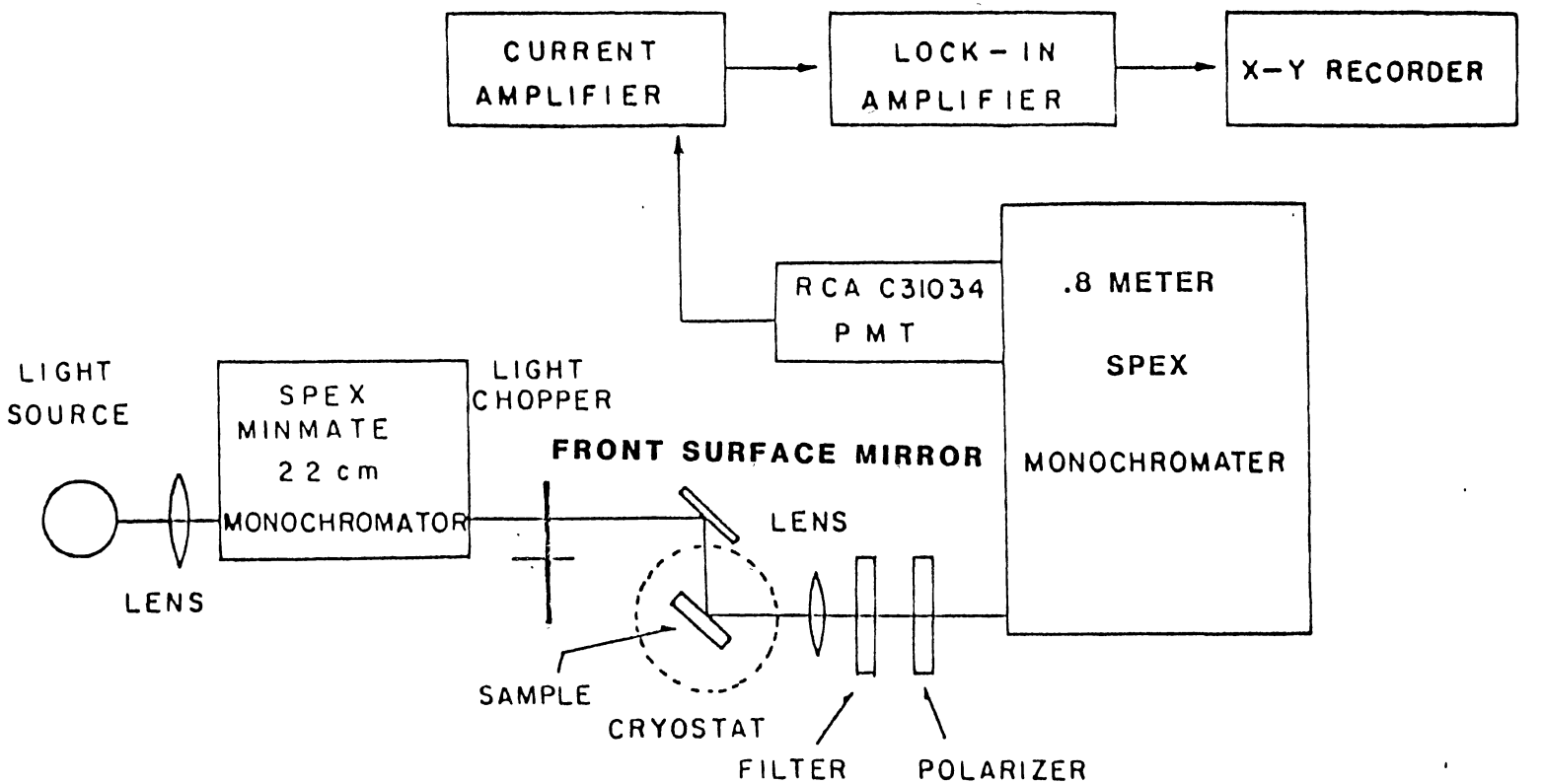

Figure 4. Block Diagram of Luminescence Apparatus

The optical excitation spectra of a luminescence band could be taken with the same apparatus described above, with the exciting light from the SPEX Minimate 22 cm monochromator driven by a synchronous motor drive. The 0.8 m SPEX monochromator was adjusted to the wavelength of the peak of the luminescence band, and the exiting light was varied from 200 nm up to the wavelength of the emission band by means of the synchronous motor drive. The intensity of the luminescence as a function of the wavelength of the exciting light was displayed on the x-y recorder. The intensity of the exciting light from the Xe lamp and minimate monochromator was measured with a Spectra Radiometer Model 301. The excitation spectra were corrected accordingly.

When necessary, sharp cut-off filters from Hoya Optics were used in the excitation of emission beam path to minimize stray light.

Life-time measurements at 300K were done by Mr. Greg J. Quarles and once more I extend my thanks to him. The apparatus used in this measurement consists of an RCA C31034 photomultiplier tube, powered by a Thorn EMI model 3000R high voltage power supply. The lifetimes were recorded by feeding the signal from the phototube into the one meg ohm input of an oscilloscope., in parallel with a variable resistor. The oscilloscope used was a Tektronix Model 7834 Storage Oscilloscope with a model 7A16A amplifier and a Model 7B92A dual time base unit that has a 0.5 ns time per division minimum scale. After making sure that there was no distortion due to the input level resistor, the storage function was used to store the lifetime on the screen and from there it was possible to calculate the appropriate lifetime.

CHAPTER III

EXPERIMENTAL RESULTS

In this chapter the details of experimental results will be presented in the logical order of findings. Along with this, the results of computer analyses will also be presented as an attempt to complete the indentification of the defect centers. In the next chapter the discussions and interpretations of the results will be given along with comparisons of these results with those of other materials.

Figure 5 displays the absorption spectrum of $RbCaF_3$ at 77K obtained after irradiation at a dose of 13.3×10^{15} MeV/cm^3. This spectrum corroborates the earlier results obtained by Seretlo, Martin, and Sonder (18) showing three major absorption peaks between 200 nm and 800 nm. There is a broad absorption band between 500 and 600 nm, a rather sharp doubly peaked band at 400-415 nm and a short wavelength band near 320 nm.

The shape of the band f 320 nm suggests that it may be actually a combination of two broad bands possibly due to two different defect centers as was also indicated in earlier work by Halliburton et al (19). To obtain an idea of what the defect centers might be and how they constitute the 320 nm band the sample was bleached with white light after irradiation. The result of bleaching showed a drastic diminution of the 530 nm band and f 320 nm band with the f 400 nm band remaining practically unchanged. This suggested that the f 320 nm band may be due

to a defect centers constituted of self-trapped holes, viz. V_k center and H-center. Now the question becomes what are the precise positions and shape of the V_k as well as H-center band. To determine this two sets of experiments were done.

In the first set of experiment the sample was given a short burst of radiation at a dose of 0.587×10^{15} MeV/cm^3 which should produce V_k centers without H-centers. Then the sample was bleached with 320 nm light with E C and E C, the crystal c-axis of the smaple being previously determined. The results of bleaching experiment show: (a) ~ 320 nm band shows dichroism, indicating that it is most probably the V_k center, and (b) ~ 530 nm band decreases indicating a possible electron trap center.

Figure 6 shows the difference of two curves, before and after bleaching with E C. The band shape of two peaks are Gaussian type. Table X shows the exact peak position and half-width of the Gaussian fits for two peaks individually. These are the peak positions and half-widths of V_k center and electron-trap center bands to be used later to construct the ~ 320 nm band and ~ 530 nm band discussed earlier.

In the second set of experiments the sample was irradiated rather heavily ($30 \cdot 5 \times 10^{15}$ Mev/cm^3) so that both V_k and H-centers are created. In order to find the necessary information about the H-center, the V_k center was bleached out completely. The absorption spectra at three different temperatures after bleaching the V_k center each time are shown in Figure 7. The shape of the bands are close enough to Gaussian to get the appropriate peak position and half-width given in Table XI.

From these two sets of experiments we get the information about the peak positions and half-widths of possible V_k center, H-center and

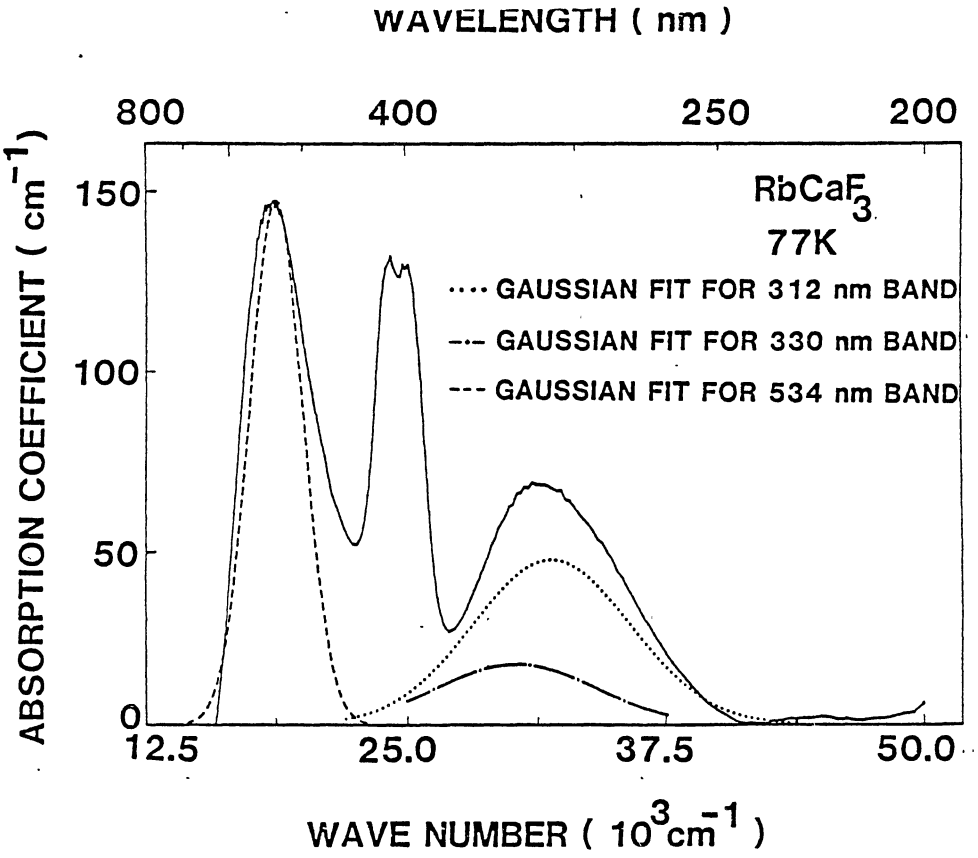

Figure 5. Absorption Spectrum of $RbCaF_3$ at 77K and Gaussian fits for 530 and 320 nm bands

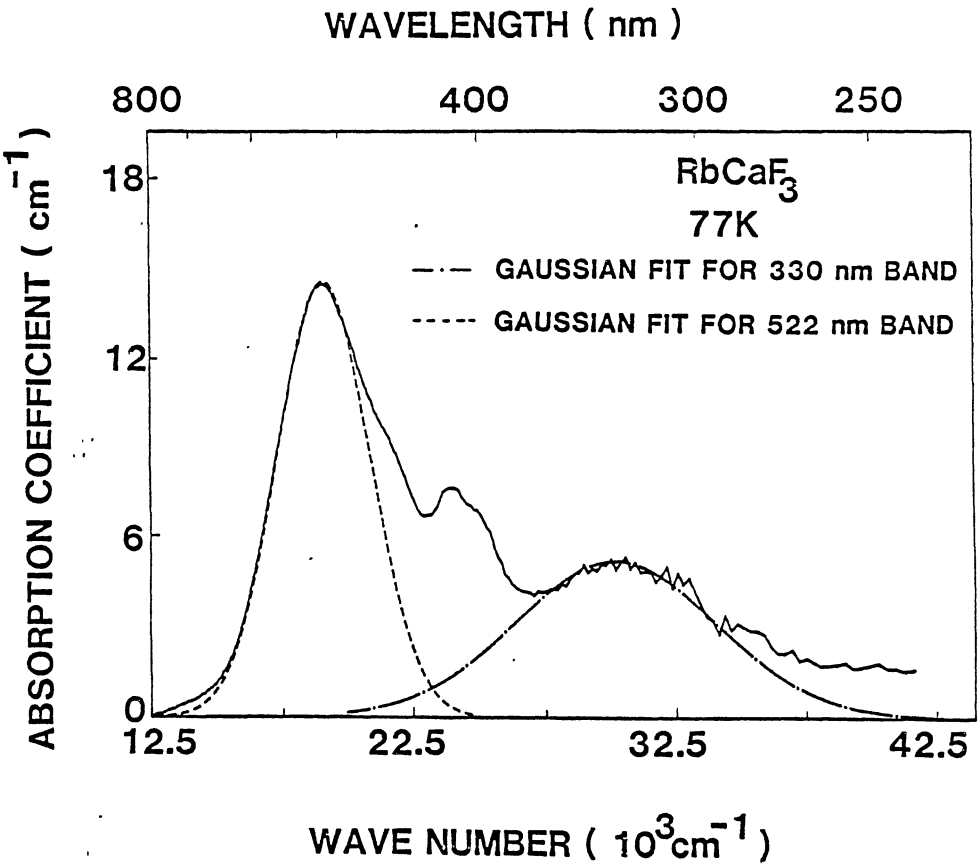

Figure 6. Difference spectrum of $RbCaF_3$ at 77K before and after bleaching and Gaussian fits for 330 and 522 nm bands

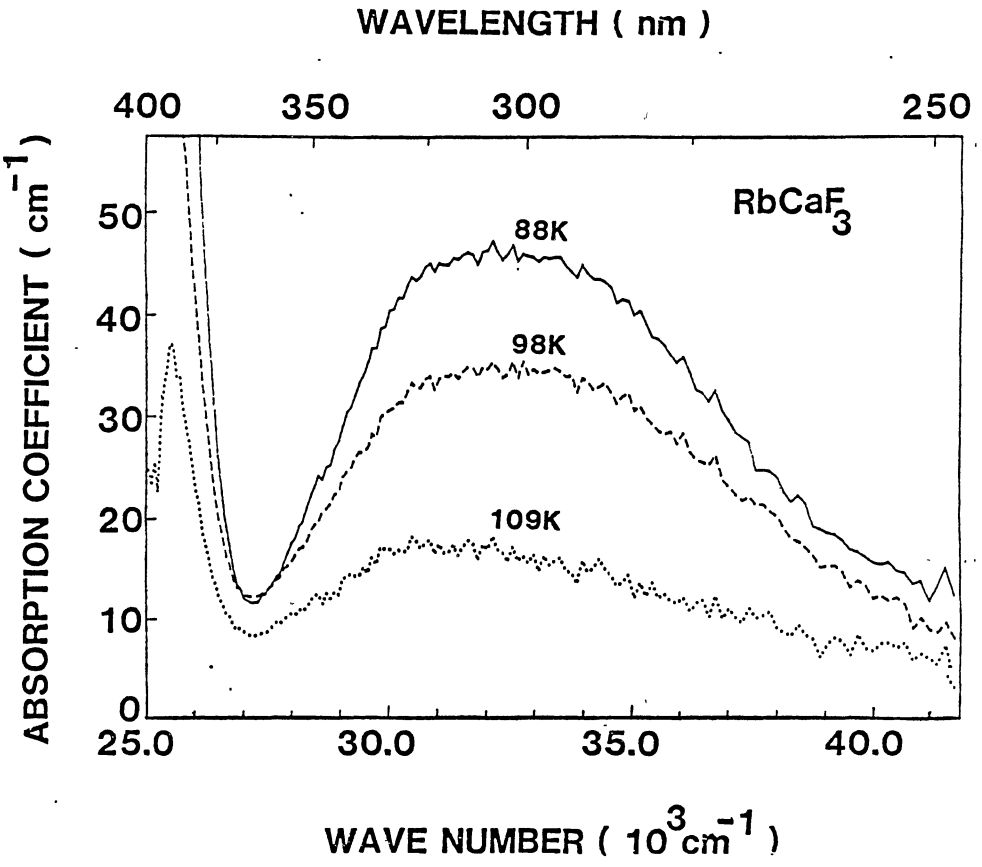

Figure 7. Absorption spectra of $RbCaF_3$ after bleaching at three different temperatures

TABLE X

THE PEAK POSITIONS AND HALF-WIDTHS FOR GAUSSIAN FITS IN FIGURE 6

Band	Peak Position		Half-width	
	nm	cm^{-1}	nm	cm^{-1}
530 nm	522	19157	2423	4126
320 nm	330	30303	1105	9047

TABLE XI

THE PEAK POSITION AND HALF-WIDTHS OF THE PEAK WITH MAXIMUM ABSORPTION COEFFICIENT IN FIGURE 7

Peak Position		Half-width	
nm	cm^{-1}	nm	cm^{-1}
312	32051	1113	8984

TABLE XII

THE PEAK POSITIONS AND HALF-WIDTHS FOR GAUSSIAN FITS IN FIGURE 5

Band	Peak Position		Half-width	
	nm	cm^{-1}	nm	cm^{-1}
530 nm	534	18727	3151	3174
	330	30303	1105	9047
320 nm	312	32051	1113	8984

electron trap bands.

With these particular peaks positions and half widths, the three main bands in the absorption spectrum shown in Figure 5 can now be constructed individually with Gaussian fits as is done in the figure. There are two Gaussian curves under the ~320 nm band. Table XII shows the peak positions and half-widths of these bands in Figure 5.

Comparing the results collected in Tables X, XI, and XII we see that the results agree exactly for V_K center and H-center bands, but both the peak positions and half-widths of the band at ~530 nm, are not exactly the same in Tables X and XII.

As we have said earlier the third major peak appears at 400 - 415 nm. The absorption spectra of this doubly peaked band for different doses are shown in Figure 8. For very low doses, there are two distinct peaks in this region. As the dose is increased the peak at longer wavelength (440nm) decays out by a small amount but the one at shorter wavelength (400nm) continues to grow with a final peak position at ~415 nm . This characteristic of the third band, therefore, suggests the possibility of two or more defect centers in this region.

Figure 9 portrays the growth rate of these bands at liquid nitrogen temperature. The band at 530 nm grows much faster than the others. It attains a maximum at a relatively small dose of 0.837×10^{15} MeV/cm^3. It then starts decreasing by a small amount with increasing radiation dose and finally becomes saturated at a dose of 8.75×10^{15} MeV/cm^3. On the other hand the double peak at 400 - 415 nm appear to be nearly saturated at a dose of 35×10^{15} MeV/cm^3. The characteritics of these two bands are similar to those observed by Seretlo et al. (18). The growth curve for the band at 320 nm has points marked by two different

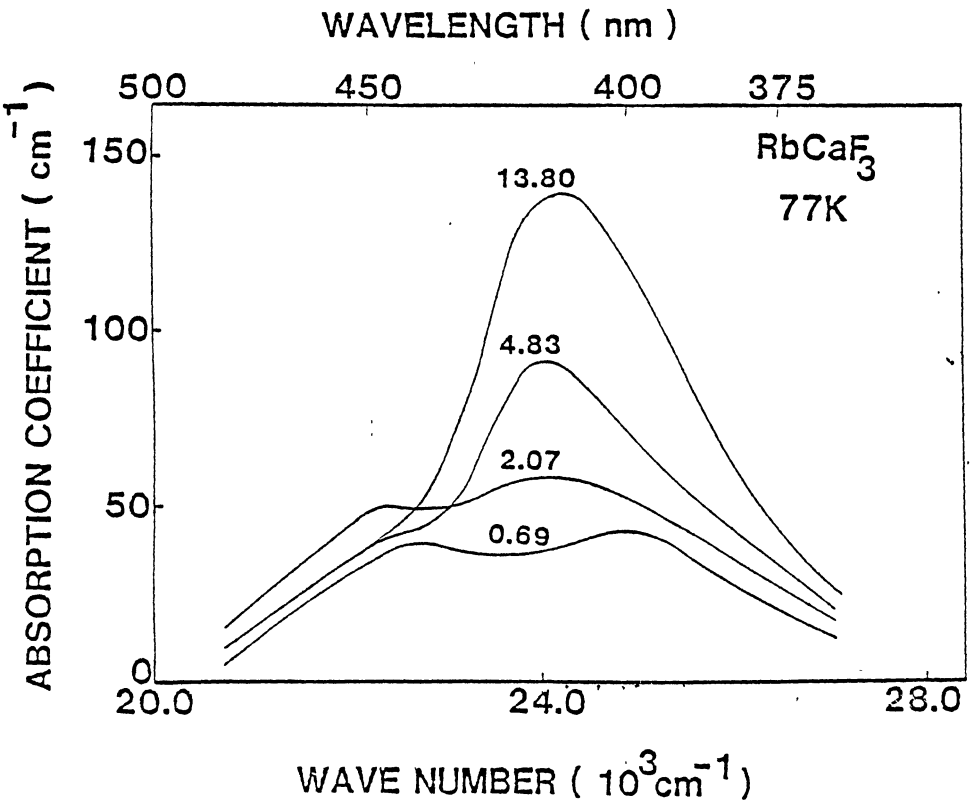

Figure 8. Absorption Spectra of $RbCaF_3$ Irradiated and Measured at 77K. The Numbers Next to the Curves Indicate the Absorbed Dose in Units of 10^{15} MeV/cm^3

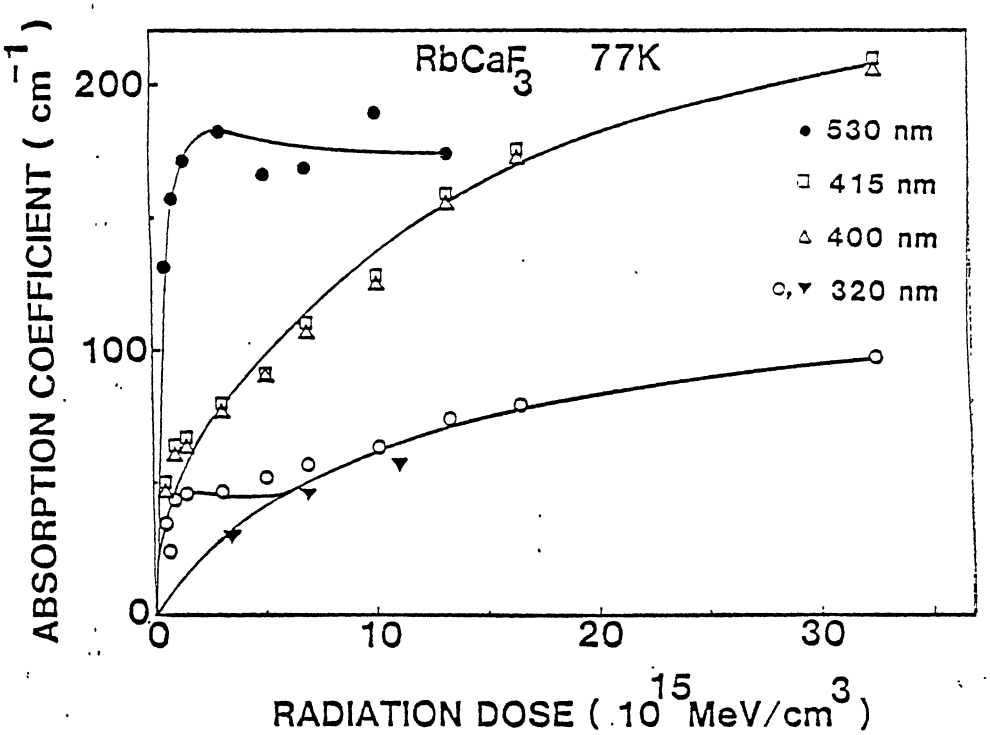

Figure 9. Growth Curves of Four Absorption Bands of $RbCaF_3$ Irradiated and Measured at 77K. o Represents Points Before Bleaching and V Represents Points After Bleaching

symbols. Points marked by circles were obtained from absorption spectra taken before the sample was bleached after irradiation, or in other words, when both V_k and H-centers are present in the irradiated sample. Points marked by full inverted triangles were obtained from the absorption spectra taken when the sample was bleached right after irradiation or in other words, when both V_k and H-centers are created but only H-centers are present in the irradiated sample. From the growth curves shown in the figure we can infer that with small radiation doses, it is the V_k center which grows rapidly and then abruptly saturates at a comparatively low doese of $.405 \times 10^{15}$ MeV/cm^3. On the other hand, H-center growth is slow but steady at small radiation doses and it continues to grow even when the V_k center growth is saturated. Finally at high enough dose it comes close to saturation. These growth characteristics of V_k and H-center defects are similar to those observed by Halliburton et al.(19).

From these growth curves it is apparent that all three main absorption regions have a consistent tendency of growth at low doses and then saturation at high doses. In this context we may point out the fact that the 530 nm band and the 320 nm band for V_k centers exhibit quite similar behaviour with respect to their growth rate and saturation. So if we assign 530 nm band as that due to electron trap centers, then the second one, viz. 320 nm and to be more precise, 330 nm band (from Figure 5) is due to self-trapped holes centers or V_k centers. Again, we may note that the growth curve for 400 nm - 415 nm band and that for H-centers, after V_k centers were bleached out, show similar behaviour with respect to their growth rate and saturation. this provides further evidence of interstitial-vacancy pair production

which suggests the 400-415 nm band be assigned to F-centers.

The growth behaviour of 400 nm band as a function of dose at three different temperatures is illustrated in Figure 10. At 77K, the band grows with dose very rapidly whereas at 6K, it grows much slower but it continues to grow as the dose is increased. At 300K only slight coloration occurs and is completely saturated at a low absorption coefficient of 10 cm^{-1} at a dose of 8.72×10^{15} MeV/cm^3. After this point the absorption coefficient is completely independent of radiation dose. From these three growth curves we note that for the same amount of dose, the absorption coefficient of F-center defects is maximum at 77K. Minimum at 300K and at 6K it has values that lie in between thse two temperatures.

As were have already seen in Chapter I, at temperatures nearer 300 K, the defects, both interstitials and vacancies, become mobile. When the vancancies become mobile, they aggregate to form F_2 centers. To detect these F-aggregate centers we irradiated the sample at room temperature (300K) and observed the absoprtion spectrum at 77K shown in Figure 11. This spectrum shows a very small peak at wavelength 570 nm. This peak at 570 nm was also observed by Seretlo et al. (17). They calculated the half-width of this band to be 0.1 ev (=806 cm^{-1}) at 77K which agrees closely with our calculated value of about 897 cm^{-1}. In addition to the small peak at 570 nm two distinct peaks at 512 nm and 415 nm and a broad hump at 450 nm are observed. The peak at 415 nm has a shoulder at 400 nm.

In order to identify possible $F_2(M)$ and $F_3(R)$ centers luminescence experiments were done with exciting light at 570 nm. the luminescence spectrum as shown in Figure 12 has two distinct peaks at 666 nm and at

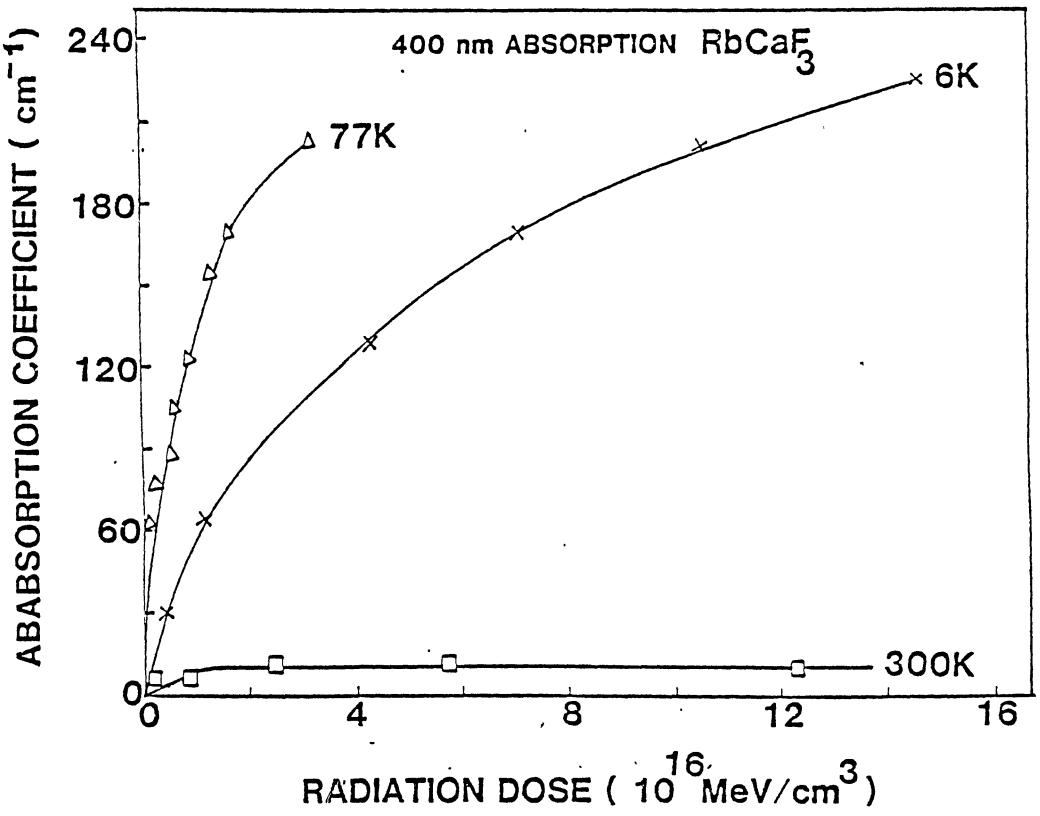

Figure 10. Growth Curves of 400 nm Band of $RbCaF_3$ Irradiated at Three Different Temperatures

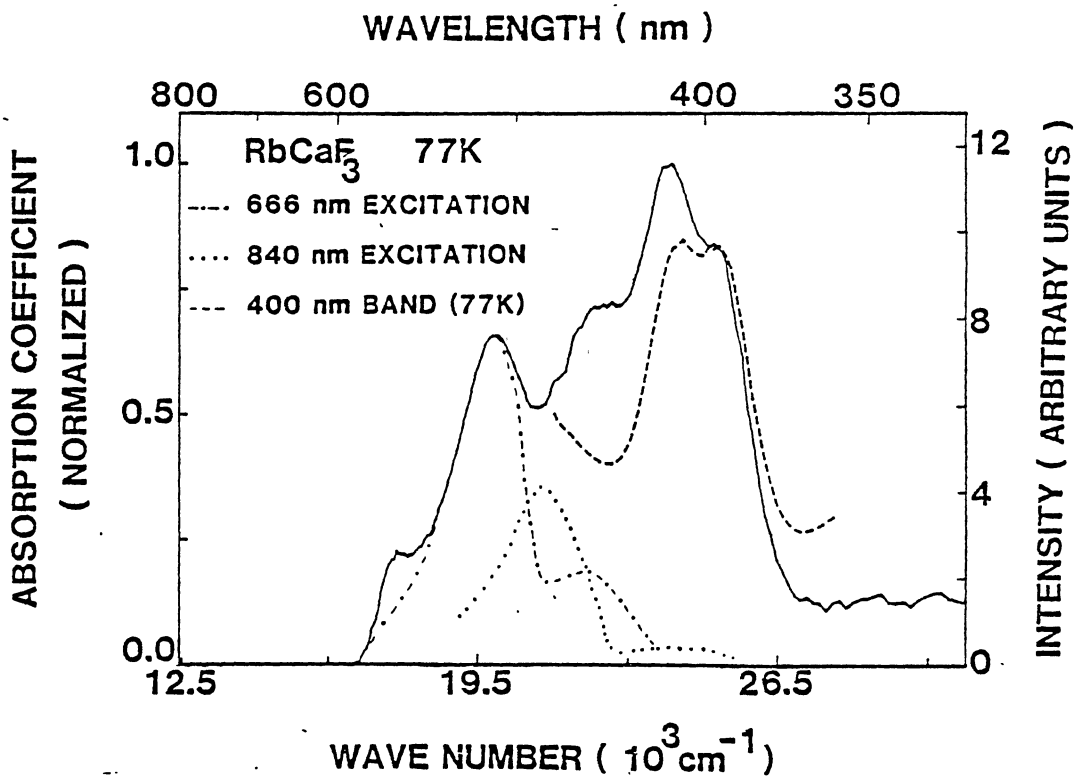

Figure 11. Absorption and Excitation Spectra of $RbCaF_3$ Irradiated at 300K, and Measured at 77K. Dotted Line is for 400 nm Band of $RbCaF_3$ Irradiated at 77K

840 nm. the excitation spectra for these two peaks are shown in Figure 11. In order to see if the absorption spectrum of the sample irradiated at 300K sample matches with the excitation spectra from these two luminescence peaks, several adjustments were made. First of all, the value at the peak intensity of the excitation spectrum for 666 nm emission band was adjusted to the value of the absorption spectrum at wavelength 512 nm. The intensity of the second excitation spectrum for 840 nm peak in the emission spectrum was adjusted so that the ratio of the relative intensities of the two spectra are maintained. From this figure we see that the 512 nm peaks appears both in absorption and in excitation spectra. But the other peaks are not the same. No emission was found with exciting light in 400 - 415nm range. Furthermore, in order to see how the 400 - 415 nm peak for low temperature (77K) irradiated sample is related with that for sample irradiated at 300K, the trace of the absorption spectrum with adjusted peak absorption coefficient at low temperature irradiated sample is superimposed on that for the sample irradiated at room temperature. From this we see that the peak at 400 nm (at 77K) matches that at 300K, but the peak at 415 nm is much more prominent at 300K than that at 77K.

Next the lifetimes for both 666 nm and 490 nm emissions were measured. The relative intensity with respect to time curves are shown in Figures 13 and 14 respectively. From these figures it is evident that the relative intensity for both inensities falls exponentially with time. Table 13 shows the lifetimes for these two peaks.

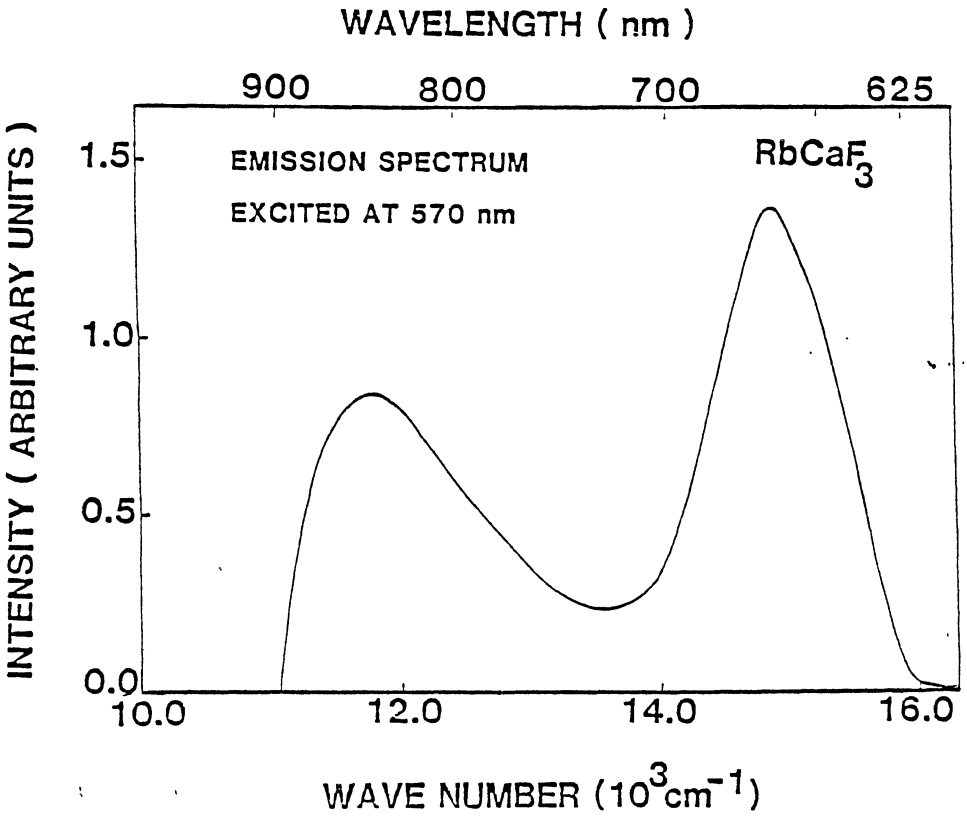

Figure 12. Emission Spectrum of $RbCaF_3$ Excited at 570 nm

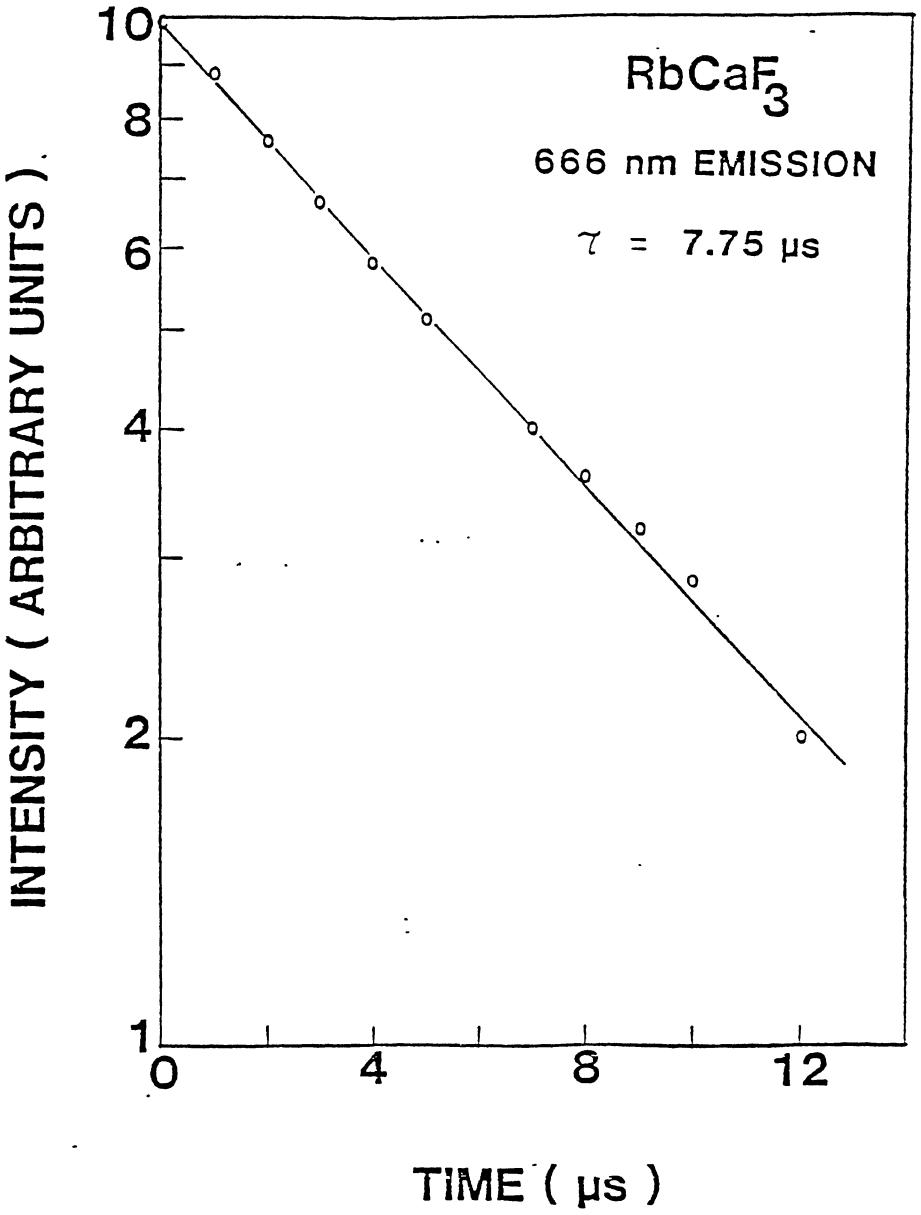

Figure 13. Change of Relative Intensity with Time of 666 nm Emission Band with Lifetime = 7.75 μs

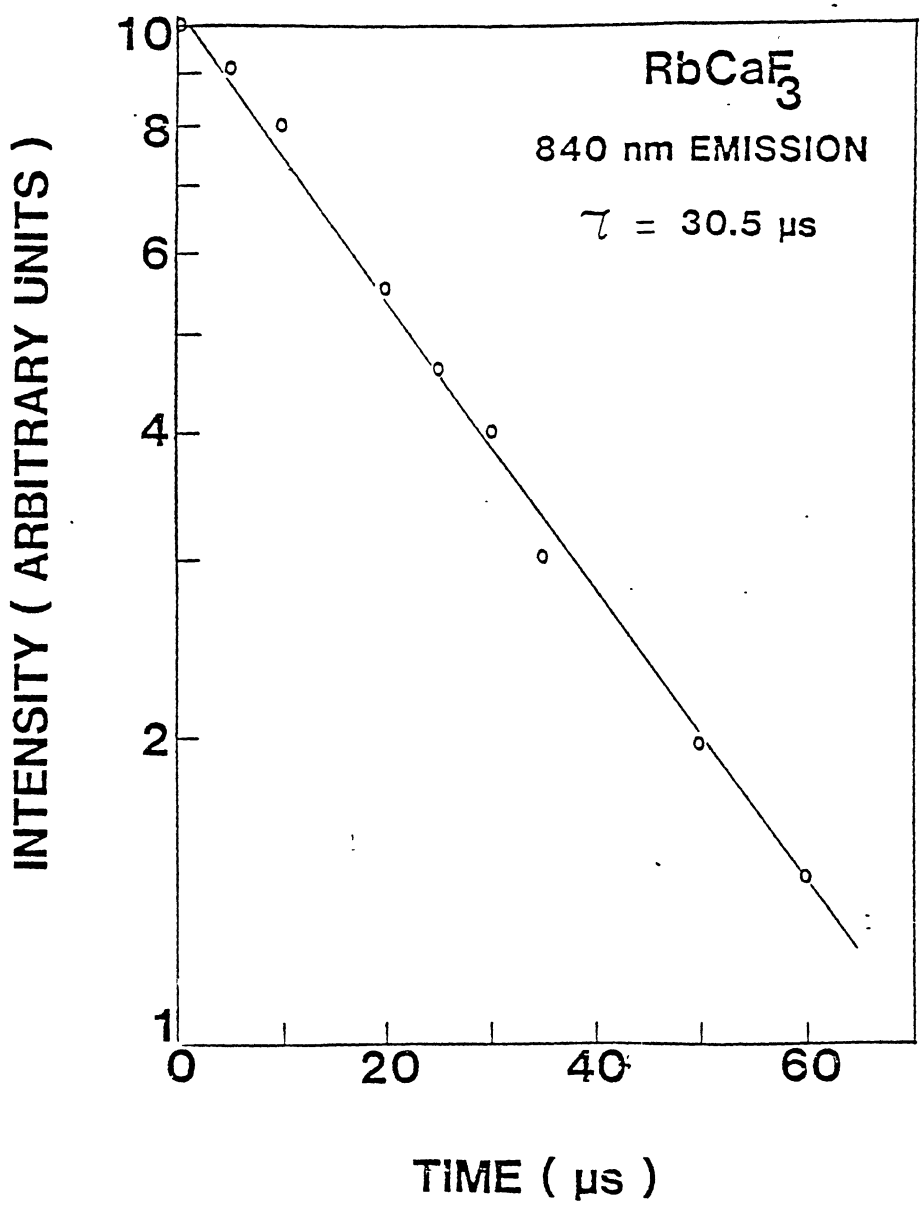

Figure 14. Change of Relative Intensity with Time of 840 nm Emission Band with Lifetime = 30.5 μs

TABLE XIII

LIFETIMES FOR 666 nm AND 840 nm EMISSION BANDS

Band Position		Lifetime	Temperature
nm	cm^{-1}	(μs)	(°K)
666	15015	7.75	300
840	11905	30.5	300

CHAPTER IV

DISCUSSION

As noted in Chapter III, the three major absorption peaks occur for $RbCaF_3$ crystal irradiated at 77K. Of them, the band at 530 nm and that at 330 nm can be assigned those due to electron trap centers and due to X_2^- (V_k) centers respectively due to their particular growth behavior. The assignment of the latter band, viz. 330 nm was further confirmed by EPR methods done by Halliburton et al. (35). We have also showed in Chapter III that the band ~ 320 nm is actually composed of two different peaks one of which is at 330 nm mentioned above and the second one is at 312 nm due to interstitial type H-center defects confirmed by the analysis of growth behaviour and also by ESR studies (19). The third major absorption peak is at 400 - 415 nm range which we tentatively assigned due to F-centers but which needs more detailed investigation.

In nearly all theoretical models for F-center absorption the potential has one consistant feature. In the region of the vacancy, the potential resembles that of a three-dimensional square well. this potential is the electrostatic potential generated by the ions in the crystal, treated as point charges. The potential energy is constant (equal to the Madelung energy, typically - 9 eV) out to around nearest neighbour distance, where it increases rapidly and oscillates as distance r increases, falling off on the average as $\frac{e^2}{r}$, where e is the

charge of an electron.

Using this infinite square well model for the potential, the energy between the ground state and the first excited state is given by,

$$E_{2p} - E_{1s} = \frac{3\pi^2 h^2}{8\ ma^2} \tag{8}$$

where 1s is the ground state, 2p the excited state and a is the distance from the origin to the potential barrier. If the difference in energy for the F-center band is written as E_F, then we have:

$$E_F = \frac{3\pi^2 h^2}{8\ ma^2} \tag{9}$$

or

$$E_F = ka^{-2}$$

where k is constant equal to $\frac{3\pi^2 h^2}{8m}$.

F-band transition energy E_F, found experimentally for various alkali halides when plotted on a log-log paper against the lattice parameter of the material; yields a straight line, the slope and intercept of which were displaced from the theoretical straight line plot represented by the above equation. The equation representing the straight line connecting the experimental data gives a relationship between E_F and a. A relation of this kind found from experimental data was first derived by Mollwo (1931) and later modified by Ivey (1947) and many others (36,37).

In Figure 15 we have plotted the peak energies for F-center bands

vs. nearest-neighbour distance for alkali halides (36). This gives a Mollwo-Ivey type relationship between the peak energies of F-band and nearest-neighbour distance with the equation of straight line given by

$$E_F = .220a^{-1.91} \tag{10}$$

In Figure 15, we have also plotted the peak energies of F-center bands vs. nearest-neighbour distance where E_F is in eV and a is in nm for alkaline earth halides like CaF_2, SrF_2, and BaF_2 (37) together with the values for $KMgF_3$ and MgF_2 (4). The peak energies (E_F) of F-center bands, in this case, are related to their nearest-neighbour distance (1) by the equation given below.

$$E_F = .0021\ a^{-4.7} \tag{11}$$

where E_F is in eV and a is in nm.

Next we have incorporated on this graph the points for $RbMgF_3$ from our data in Chapter I and those for $RbCaF_3$ which we have found experimentally in Chapter II. From the graph we can see that the data point for $RbCaF_3$ fits the second straight line far better than the one for $RbMgF_3$. In fact this point lies very close to CaF_2 data point, (Figure 15), which suggests that $RbCaF_3$ has properties similar to those of CaF_2 rather than to those of $RbMgF_3$.

Further evidence of this fact can be established if we tabulate the results of absorption and emission bands of CaF_2, $RbMgF_3$ and $RbCaF_3$ as we have done in Table XIV. The peak positions and half-widths of V_K, H and F-center bands of $RbCaF_3$ were obtained from absorption spectra and

growth behavior of absorption bands when the sample was irradiated at 77K. The peak position of F_2(M) center was found at 509 nm from the absorption spectrum (Figure 11) and measured at 77K of the sample irradiated at 300K. The assignment of the M center was further confirmed by the excitation spectrum given by 666 nm emission band which matches the absorption spectrum at 509 nm. The other peaks of the absorption spectrum cannot be well explained, as a result, no peak position for F_3(R) center can be assigned and the broad hump at 450 nm can only be suggested to be due to some perturbed F or M centers.

Comparing the peak positions and half-widths of absorption bands for different defect centers given in Table 14, we see that the peak positions of $RbCaF_3$ for different defect centers are closer to those of CaF_2 rather than to those of $RbMgF_3$, although we cannot state the same thing for half-width values. The reason for this similar behavior of $RbCaF_3$ and CaF_2 rather than $RbCaF_3$ can be attributed to the fact that in $RbCaF_3$; Ca^{2+} is much bigger in size than Mg^{2+}. The Mollowo-Ivey relationship (Figure 15) suggests that the interionic distance (2.23Å) between Ca^{2+} ion and F^- ion is the key factor in determining the transition energy of F band, rather than the interionic distance (3.13Å) between Rb^+ and F^- ions. Although in the previous discussion of the potential, the ions were assumed to be point charges, the appreciable change in size of the nearest-neighbour ions causes a significant change in the short-range potential. The same is true in case of MgO when compared with CaO. For the same resaon, E_F value of $RbMgF_3$ as is seen in Figure 15, has a higher energy shift compared to the one for $RbCaF_3$, where Rb^+ ions act only in covalent bonding without any significant effect on the transition energies from anion vacancies in these materials.

TABLE XIV

TABLE FOR PEAK POSITONS AND HALF-WIDTHS FOR DIFFERENT DEFECT CENTERS OF CaF_2, $RbMgF_3$ and $RbCaF_3$

Defect Center	Peak Position in cm^{-1}			Half-Width in cm^{-1}		
	CaF_2	$RbMgF_3$	$RbCaF_3$	CaF_2	$RbMgF_3$	$RbCaF_3$
V_k	30675	30303	30303	8000	7655	9047
H	33333	-	32051	7000	-	8984
F	26596	-	25000	1.11×10^5	-	?
$F_2(M)$	19194	25840	19863	4.77×10^5	1813	2000
$F_3(R)$	14567	33333	?	270	2417	?

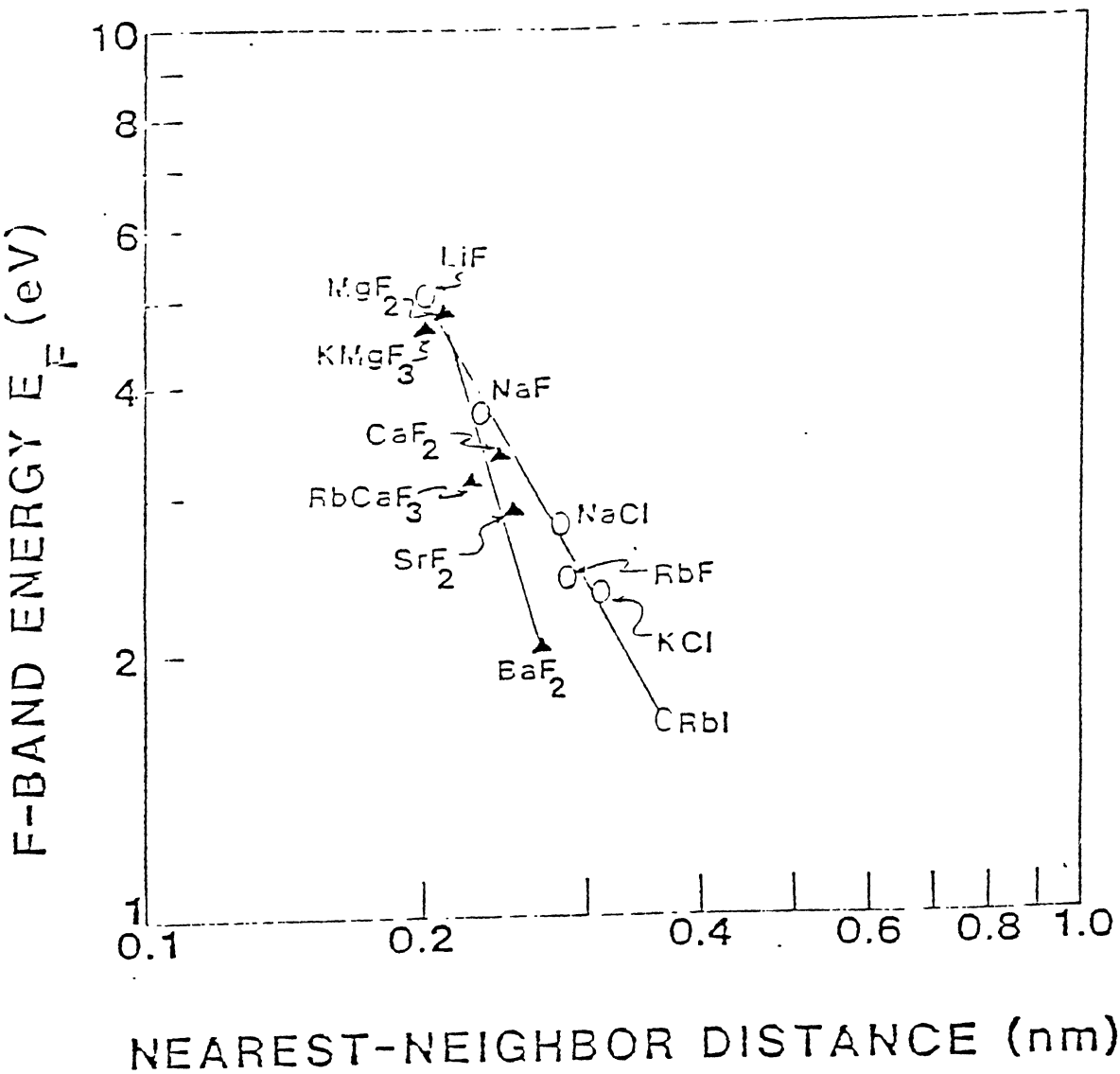

Figure 15. The Mollwo-Ivey Relationship Between F-Band Peak Energies and Nearest-Neighbor Distance from Some Halides

CHAPTER V

SUMMARY AND SUGGESTION FOR FURTHER STUDY

Samples of $RbCaF_3$ have been irradiated at 77K with electrons from a Van de Graff accelerator to produce defects in the crystal. These defects include self-trapped hole centers like V_k and H centers, electron trapped in anion-vacancy (F) type centers and electron trap centers. The absorption bands due to these defects and their growth curves as a function of dose were studied. After irradiation the sample was bleached from a mercury source due to which V_k and electron trap centers are reduced by a great amount. After analysing the difference curve exact peak position and half-width of V_k center band was determined. On bleaching V_k center absorption band, the absorption band due to H-center was singled out; the peak position and half-width of which was then determined.

The growth behavior of different absorption bands further confirmed the assignment of different defect centers. The growth behavior of the F-center absorption band was studied at 6K, 77K and 300K. The absorption spectrum of the sample irradiated at 300K and measured at 77K was taken to facilitate the study of F-aggregate centers like $F_2(M)$ and $F_3(R)$ centers. It was observed that two emission peaks (666 nm and 840 nm) are produced by a defect which absorbs light at 570 nm. The excitation spectrum obtained from 666 nm emission band matches the peak in absorption spectrum at 590 nm suggesting it to be due to $F_2(M)$

centers. The other peaks in the excitation spectra are not well-matched to those in absorption spectra. The absorption spectrum reveals a peak in the same position as that observed due to F-center band for the low-temperature (77K) irradiated crystal. The rest of the absorption bands in the absorption spectrum cannot be well explained except some suggestion that the one at 450 nm may be due to some perturbed $F_2(M)$ or F-centers.

Lifetime data for two emission peaks were also taken. The lifetime for one them (666 nm) is too short for further study of temperature dependence. The lifetime for the second one (840 nm) can be further studied for temperature dependence. So the most obvious next step for further study is to observe the temperature dependence of lifetime of this emission band. This may give some idea about the energy transfer process occurring in the crystal. At the same time, the temperature dependence study of the half-width of this emission band can be used to calculate the phonon mode frequency and the Huang-Rhys factor. Although no zero phonon line has been observed so far, the value of Huang-Rhys factor will indicate the possibility of one, if there is any.

Further, the thermal annealing experiments for H-center defects can be done to see if the results agree with previous work (19). Annealing experiments can also be done for V_k center defects after irradiating the crystal with x-rays. The x-ray fluorescence experiments can also be performed as was done with CaF_2 to compare the results for the two crystals as was done with other defect centers in the present study.

$F_2(M)$ and $F_3(R)$ centers need to be studied more thoroughly. Although no absorption band has been found for $F_3(R)$ centers so far for $RbCaF_3$, $F_3(R)$ centers has been found in CaF_2. So the absorption

spectrum for the sample irradiated at high temperature should be studied more extensively, possibly in conjunction with different directions of polarizations. A search involving electron spin resonance (ESR) techniques would help to determine more precisely the positions of $F_2(M)$ and $F_3(R)$ centers.

Finally, studies of defects in $RbCaF_3$ crystal doped with ions like Mn, Ni, Co, and Fe would yield further information about these defects. It is possible that impurities in the supposedly pure crystal used in this study are responsible for some of the characteristics observed in this study. Since significant results are available from doped samples, studies of such doped crystals need to be done to allow for adequate comparison. Also the perturbing effect of the impurity ion upon the defect may improve certain characteristics such as lifetime so that such a crystal would be better suited for practical applications.

REFERENCES

1. Nassau, K., Sci. Am., 243, 124 (1980).

2. Podnish, A. and W.A. Sibley, Phys. Rev. B, 18, 5921 (1978).

3. Sibley, W.A. and N. Koumvakalis, J. Phys. C, 10 4909 (1977).

4. Koumvakalis, N. and W.A. Sibley, Phys. Rev. B, 13, 4509 (1976).

5. Hall, T.P.P. and A. Leggeat, Solid State Commun. 7, 1651 (1969).

6. Riley, C.R. and W.A. Sibley, Phys. Rev. B,1 2789 (1970).

7. Riley, C.R., S.I. Yun, and W.A. Sibley, Phys. Rev. B, 5, 3285 (1972).

8. Sibley, W.A., and O.E. Facey, Phys. Rev. 174, 1076 (1968).

9. Sibley, W.A. IEEE Trans. Nucl. Sc. NS-18, 273 (1971).

10. Beaumont, J.H., W. Hayes, D.L. Kirk, and G.P. Summers, Proc. Roy. Soc., Lond. A, 315, 69 (1970).

11. Atobe, K., M. Okada and M. Nakagawa, Rad. Effects 32, 155 (1977).

12. Beaumont, J.H. and W. Hayes, Proc. Roy. Soc. Lond. A, 309, 53 (1969).

13. Beaumont, J.H., A.L. Harmer, and W. Hayes, J. Phys. C, 5, 1457 (1972).

14. Beaumont, J.H., A.L. Harmer, and W. Hayes, J. Phys. C, 5, 275 (1972).

15. Pauling, L. Nature of the Chemical Bond (Cornell University Press, Ithaca, 1945)

16. Martin, J.J., G.S. Dixon, and P.P. Valesco, Phys. Rev. B. 14, 2609 (1976).

17. Ho, J.C. and W.P. Unruh, Phys. Rev. B. 13, 447 (1976).

18. Seretlo, J.R., J.J. Martin, and E. Sonder, Phys. Rev. B. 14, 5404 (1976).

19. Halliburton, L.E., A. Jafari and R.A. Burris, Phys. Rev. B 23, 6765 (1981).

20. Bulou, A., C. Ridou and M. Rousseau, J. Nouet and A.W. Hewat, J. Physique 41, 89 (1980).

21. Modine, F.A., E. Sonder, W.P. Unruh, C.B. Finch and R.D. Westbrook, Phys. Rev. B 10, 1623 (1974).

22. Hensley, E.B., W.C. Ward, B.P. Johnson and R.L. Kores, Phys. Rev. 175, 1227 (1968).

23. Schulman, J.H. and W.D. Compton, Color Centers in Solids (Macmillan, New York, 1962)

24. Sonder E. and W.A. Sibley, In Point Defects in Solids, edited by J.H. Crawford and L.M. Slifkin (Plenum, New York, 1972).

25. Pooley, D. and W.A. Sibley, In Color Centers and Radiation Damage, Research Group Report, Materials Development Division, Atomic Energy Research Establishment, Harwell, Berkshire (1973).

26. Castner, T.G. and W. Kanzig, J. Phys. Chem. Solids 3, 178 (1957).

27. Woodruff, T.O. and W. Kanzig, J. Phys. CHem. Solids 5 268 (1958).

28. Delbecq, C.J., W. Hayes and P.H. Yuster, Phys. Rev. 121, 1043 (1961).

29. Jones, G.D. Phys. Rev 150, 539 (1966).

30. Murray, R.B. and F.J. Keller, Phys. Rev. 153, 993 (1967).

31. Hobbs, L.W., A.E. Hughes and D. Pooley, (1972) AERE-R6953 (also Phys. Rev. Lett. 29, 234 (1972))

32. Pooley, D. Proc. Phys. Soc. 87, 245 and 257 (1966a)

33. Pooley, D. Proc. Phys. Soc. 89, 723 (1966b)

34. Pooley, D. J. Phys. C. 1, 323 (1968).

35. Halliburton, L.E. and E. Sonder, Solid State Communications, 21, 445 (1977)

36. Dawson, R.K. and D. Pooley, Phys. Status Solide B 35 95 (1969).

37. Turner, Thomas J. Solid State Communications, 7, 635 (1969)

VITA V

Rina Chakrabarti

Candidate for the Degree of

Master of Science

Thesis: OPTICAL ABSORPTION AND EMISSION FROM RADIATION DEFECTS IN $RbCaF_3$

Major Field: Physics

Biographical:

Personal Data: Born in Calcutta, India, January 16, 1961.

Education: Graduated from Bethune Collegiate School, Calcutta, India, in May 1978; graduated from the University of Calcutta in May, 1981 with Bachelor of Science degree with first-class Honors in Physics; completed B. Tech. part I degree in Computer Science, with first class from University of Calcutta, in July, 1983; completed requirements for the Master of Science degree at Oklahoma State University in December 1985.

Professional Experience: Teaching and Research Assistant from January 1984, to July 1985 at Oklahoma State University.